SARS-CoV-2 spike antibodies cross-react with dengue virus and enhance infection *in-vitro* and *in-vivo*

Kamini Jakhar[1†], Sudipta Sonar[1†], Gagandeep Singh[2], Tejeswara Rao Asuru[3†], Garima Joshi[3†], Nisha Beniwal[1], Tania Sarkar[1], Mahima Tiwari[1], Jaskaran Kaur[1], Deepak Kumar Rathore[4], Banwari Lal[1], Sandeep Kumar[1], Puneet Srivastav[1], Satendra Kumar[1], Vikas Phagna[1], Sushma[1], Lokesh Kumar[1], Vishal Gupta[1,5], Pallavi Kshetrapal[6], Savita Singh[6], Nitya Wadhwa[6], Ramachandran Thiruvengadam[6,7], Sreevatsan Raghavan[6], Mudita Gosain[6], Tripti Shrivastava[1], Sankar Bhattacharyya[1], Shailendra Asthana[2], Prasenjit Guchhait[3] and Shailendra Mani[1#]

† Contributed equally

#Corresponding author

Corresponding author: Shailendra Mani, PhD.

Email: shailendramani@thsti.res.in

Author affiliations:

1. Centre for Virus Research, Therapeutics and Vaccines, Translational Health Science and Technology Institute, Faridabad, Haryana, India-120001
2. Computational Biophysics and CADD group, Computational and Mathematical Biology Centre (CMBC), Translational Health Science and Technology Institute (THSTI), Faridabad, Haryana, India-120001
3. Regional Centre for Biotechnology, Faridabad, Haryana, India-120001
4. Centre for Immunobiology and Immunotherapy, Translational Health Science and Technology Institute, Faridabad, Haryana, India-120001
5. Translational Health Science and Technology Institute, Faridabad, Haryana, India-120001

6. Centre for Maternal and Child Health, Translational Health Science and Technology Institute, Faridabad, Haryana, India-120001
7. Department of Biochemistry, Pondicherry Institute of Medical Sciences, Kalathumettupathai, Ganapathichettikulam Village No.20, Kalapet, Puducherry, India-605014.

Word Count

Abstract- 140

Main text- 3433

Abstract:

The presence of non-neutralizing antibodies of any dengue serotype, increase the severity of subsequent infection by other dengue serotypes. During SARS-CoV-2 pandemic, the number of symptomatic dengue cases increased in India. The cross-reactivity of dengue with SARS-CoV-2 is well reported. We investigated the potential of SARS-CoV-2 spike antibodies to modulate dengue infection. *In-silico* and *In-vitro* studies revealed protein-protein interactions between the spike antibodies and the dengue envelope protein. Convalescent plasma from COVID-19 patients and SARS-CoV-2 monoclonal/polyclonal antibodies showed cross-reactivity and impact on dengue infection in cell-based assays. Furthermore, increased dengue viral load was observed in serum, liver, and spleen of mice coinfected with dengue and SARS-CoV-2, compared to only dengue infected animals. Collectively, we demonstrate that SARS-CoV-2 spike antibodies can cross-react with and enhance dengue infectivity. These findings have significant implications for SARS-CoV-2 monitoring and patient management in dengue-endemic regions.

Keywords: SARS-CoV-2; Dengue Virus; Cross-reactivity; Antibody-Dependent Enhancement; AG129 Mice model

53 **Introduction**

54 Dengue is endemic to more than 120 countries with Asia contributing 70% of the global burden
55 (1). Dengue virus (DENV) circulates as four serotypes (DENV 1-4) each containing multiple
56 distinct genotypes. DENV infection can cause mild fever or lead to severe forms like Dengue
57 Haemorrhagic Fever (DHF) and Dengue Shock Syndrome (DSS). Primary infection provides
58 lifelong immunity to homotypic secondary infection but gives partial immunity from
59 heterotypic challenge. Heterotypic secondary infections present with severe symptoms, due to
60 higher viremia catalyzed by Antibody-dependent Enhancement (ADE). Sub-neutralizing
61 antibodies that bind to heterotypic DENV promote FcR-mediated viral entry into cells (2). A
62 stable attachment to Fc receptors by these antibodies, without reaching the neutralization
63 threshold leads to ADE (3).

64 The dynamics of DENV infections during the SARS-CoV-2 pandemic vary globally. A 16%
65 decline in dengue incidences was reported in 2020-21 compared to pre-COVID-19 (4).
66 However, S. Khan *et. al.* revealed a substantial surge in dengue cases in 2021 in specific South
67 Asian countries, including India (~3-fold), Pakistan (>7-fold), and Bangladesh (>19-fold). This
68 contrasted with a noteworthy decline of about 36% across Southeast Asia and Latin America
69 (5). Several regional, environmental, and pandemic-related elements have been reported to
70 shape these intricate dynamics. Disruptions in routine mosquito vector surveillance and control
71 programs during COVID-19 lockdowns may have led to a rise in dengue cases, highlighting
72 the crucial role of vector control in disease prevention. Similar pathology of DENV and
73 COVID-19 presented diagnostic challenges, potentially contributing to underreporting (4) (6)
74 (7) (8) (9).

75 Some studies indicate that ADE due to prior SARS-CoV-2 infection may elevate the risk of
76 symptomatic and/or severe dengue. In Pakistan, a significant increase in dengue-related deaths
77 (linked to DENV-2 prevalence) was observed in patients with a pre-exposure to SARS-CoV-2

78 (10). In North India, individuals with a history of COVID-19 faced a twofold higher risk of
79 developing symptomatic dengue (11). Further, the individuals vaccinated against or recovering
80 from COVID-19 exhibited higher odds (~ 3.6 times) of developing symptomatic dengue than
81 those without a COVID-19 infection or vaccination history (11).
82 Modest serological cross-reactivity between SARS-CoV-2 and DENV-2 has been reported (12)
83 (13) (14). However, it is unclear if this would have any clinical impact on dengue cases (15). A
84 study reported rabbit IgG against purified SARS-CoV-2 S1-RBD cross-reacts with DENV
85 Envelope (E), precursor-membrane (PrM), and Non-structural protein 1 (NS1). However, these
86 antibodies did not enhance DENV infection in THP-1 cells expressing FcR. Moreover, they
87 impeded DENV infection at high concentrations (16). Another study showed *in-vitro* inhibition
88 of dengue infection by sera from convalescent COVID-19 patients' sera (17).
89 Nath *et. al.* demonstrated serological cross-reactivity of SARS-CoV-2 positive serum samples
90 with DENV1 and that the sera neutralized DENV1 (17). Anti-S1-RBD antibodies were shown
91 to impede DENV infection at a specific concentration and COVID-19 patients' sera exhibited a
92 neutralizing ability against dengue infection (16). El-Qushayri *et al.,* in their systematic review,
93 aimed to assess the clinical outcomes of patients with dengue and COVID-19 co-infection. They
94 reported a high mortality rate in co-infected patients (19.1%), significantly exceeding the
95 estimated global mortality rates for dengue (1.3%) and COVID-19 (2.04%). Also, they found
96 that the hospital stay duration for co-infected individuals was longer than the reported median
97 stays for standalone COVID-19 and dengue cases (18). Although, insightful, more information
98 on the stoichiometry of the virus and antibodies in these studies, would have been useful, since
99 it is crucial for understanding antibody-virus interactions and the potential for ADE
100 Here, we evaluated the effect of preexisting SARS-CoV-2 antibodies on DENV-2 infection
101 using cell-based assays and mouse model of DENV infection.
102

103 **Results:**

104 ***In-silico* interaction mining drive the cross-recognition of DENV-E protein by anti-Spike**
105 **and anti-RBD SARS-CoV-2 antibodies**

106 To assess the cross-reactivity of SARS-CoV-2 Spike antibodies with DENV-2 E-protein dimer
107 we used an *in-silico* approach (Fig. 1A, B). We selected a panel of reported SARS-CoV-2
108 antibodies, based on their structure data (extent of their characterization, availability of the
109 structure information of their co-crystals with low resolution, preferably below 4 A°.) and
110 biological relevance (neutralization potential against SARS-CoV-2, target epitopes, etc.; Table-
111 S1). For the identification of DENV-2 E epitopes, C8 antibody against E-protein dimer (Fab
112 region, PDB-id: 4UTA) was used to characterize the interaction site based on interaction
113 fingerprinting. For identifying the cross-reactive antibodies forming the most promising
114 complexes with the E-protein; selected SARS-CoV-2 antibodies' protein-protein (PP) blind
115 docking was carried out with the whole DENV-2 E dimer. The consensus docked poses
116 obtained from Piper and HDOCK tools were used for post-docking qualitative and quantitative
117 analysis (pose selection and pose-filtering criteria). The top three SARS-CoV-2 antibodies
118 forming the complexes with DENV-2 in terms of docking energy, interaction fingerprinting
119 with co-crystal and MM-GBSA scores are CR3022 (Fab region, PDB-id:6W7Y), S2E12 ab
120 (Fab region, PDB-id:7K45) and DMAb 2196 (Fab region, PDB:8D8R) (Fig. 1C).

121 To quantitate their binding association at the residue level, major contributing amino acids were
122 identified by residue-wise decomposition analysis setting the cut-off value of -1·5 kcal/mol.
123 For the C8 antibody (4UTA) binding with DENV-2 E-protein, the interacting epitopes were
124 majorly localized in Domain II (Fig. 1D). The binding sites of CR3022, S2E12 ab, and DMAb
125 2196 antibodies were found to overlap with C8 binding site (Fig. 1D). The contributing residues
126 for all three antibodies were majorly located in Domain II including Fusion loop (Figure 1E,
127 F). The findings of overlapping residues between C8 and the three SARS-CoV-2 interacting

128 antibodies corroborate well with previously reported study (19). From the interaction analysis,
129 the R73 appeared as the most common interacting residue in all antibodies. The pair-wise
130 interaction analysis confirmed considerable overlapping residues between SARS-CoV-2 and
131 DENV-2 antibodies (Figure 1E and 1F). Key residues that overlap between DENV-2 and at
132 least two antibodies of SARS-CoV-2 are R73 (common among all), T70, S72 (Domain-II), R99
133 and N103 (Fusion loop) and E311 (Domain-III). We also performed the mining of paratope
134 residues of SARS-CoV-2 antibodies with equal and/or increased interaction energy as C8 and
135 identified overlapping residues between C8 and CR3022 (Figure S1).
136 Overall, the interaction maps and per-residue energetic decompositions showed that there were
137 several common residues involved in the interaction of DENV-2-E with C8 and CR3022,
138 S2E12 ab and DMAb 2196 antibodies indicating a high likelihood of cross-reactivity (Figure
139 1G and 1H, Table S2). The paratope residues involved in interaction of E-protein with CR3022
140 were also identified (Table-S3) and their interactions were assessed (Fig. S2).
141
142 **SARS-CoV-2 spike antibody cross-reactivity with DENV-2 and enhancement of DENV**
143 **infection**
144 Based on the computational outcomes, one of the antibodies, CR3022, which showed the
145 highest affinity with DENV-2 E protein, was studied further. Confocal microscopy images of
146 CR3022 showed a statistically significant cross-reactivity with an average Mean Fluorescence
147 Intensity (MFI) of 7·68 (p-value<0·0001) (Fig. 2A). Bio-Layer Interferometry (BLI), showed
148 high affinity with a dissociation constant (KD) of <1·0pM with Spike protein (Fig. 2B(i)), and
149 2·83 μM with DENV-2 E-protein (Fig. 2B(ii)). Further, we observed a significant augmentation
150 in the percentage of infected cells with CR3022 antibody (p-value=0·01) in comparison to
151 untreated virus control (Fig. 2C).
152

153 **SARS-CoV-2 convalescent plasma enhances DENV infection *in-vitro***

154 Samples from convalescent COVID-19 patients (n=48, Table-S4) from different time intervals
155 of the pandemic were tested for their ability to cause ADE. We used FcγR-I, II and III
156 expressing K562 and U937 cell lines. Both cell lines were shown to predominantly express
157 FcγR-II (Fig. S3), as reported previously (20). The DENV-2 infected K562 cells were observed
158 to increase from 1 to 236 times in the first set of convalescent samples (recovered individuals
159 during Wuhan wave), 77 to 235 times in the second set of convalescent samples (recovered
160 individuals during/around the delta wave), and 44 to 172 times in the third set of convalescent
161 samples (recovered individuals during omicron wave), compared to untreated virus control
162 (Fig. 3A-D). The FACS gating strategy is given in Fig. S4. Using a subset of the convalescent
163 plasma samples (n=15) similar results were observed in U937 cells, where DENV-2 infection
164 was enhanced in the range of 32 to 292 times as compared to the virus control (Fig. S5A-B). A
165 virus neutralization assay with SARS-CoV-2 Wuhan strain (Table-S5), did not show any
166 association between the neutralizing antibody titer and the ADE titers (Fig. S6A-C). Similarly,
167 we did not find any association of ADE titers with disease severity in patients with COVID-19
168 (Fig. S6D).

169 A representative quantitative PCR assay for intracellular DENV-2 genomic RNA showed a
170 higher viral load in 70% of COVID-19 convalescent plasma treated samples as compared to the
171 control (Fig. S7). This data correlates with the increase in DENV-2 positive cells observed in
172 flow cytometry. Determination of the infectious titer of DENV produced from infected cells by
173 focus-forming unit assay also showed a significant increase in the Foci-forming units/ml
174 (FFU/ml) in COVID-19 convalescent plasma treated samples as compared to control (Fig. S8).

175

176

177

178 **SARS-CoV-2 enhances dengue virus infection in mice**

179 To validate the *in-vitro* and *in-silico* findings, we carried out animal experiments. We took 21
180 AG129 mice within 6-8 weeks age group. The mice were divided into three groups, Group 1 as
181 mock (G1, N=5), Group 2 as dengue viral control (G2, N=8), and Group 3 as test with both
182 SARS-CoV-2 and dengue viral infection (G3, N=8). G2 was infected with dengue virus
183 infection at day 21. G3 was infected with SARS-CoV-2 virus at day 0 followed by dengue virus
184 infection at day 21. Both G2 and G3 mice were infected with adeno-ACE-2 (Ad5CMVh, The
185 University of Iowa Viral Vector Core Facility) viral vector at -5 days which is essential for
186 SARS-CoV-2 infection. Body weight was observed for all the animals till day 27 when they
187 were euthanized as shown in the schematic experimental plan (Fig. 4A). Average body weight
188 in G2 mice group decreased at day 3 but it recovered with time (Fig. 4B). A significant decrease
189 of body weight was observed in G3 as compared to G2.

190 We further tested the antibody response against SARS-CoV-2 spike antigen at day 21 before
191 SARS-CoV-2 infection, we observed the anti-spike IgG antibody response in all mice in G3
192 (Fig. 4C). We next determined the live dengue virus particle in serum samples collected on day
193 27 (Fig. 4D), we observed a slightly higher number of viral particles in G3 as compared to G2
194 indicating enhancement of Dengue infection with SARS-Co-V-2 virus. Next, we tested the viral
195 replication in the liver and spleen of the infected mice. We observed a high copy of viral RNA
196 both in liver (Fig. 4E) and spleen (Fig. 4F) tissues. We also observed a decrease in the platelet
197 count, as previously reported to occur during dengue infection. As shown in Fig. 4G, a decrease
198 in the platelet count was seen in G1 vs G2 and G3 however, we did not observe any significant
199 difference in G2 vs G3. WBC and Hematocrit measurement was also carried out but no
200 significant differences in G2 vs G3 groups (Fig. 4H & 4I) were observed.

201

202

203 **SARS-CoV-2 spike antibodies cross-react with DENV**

204 SARS-CoV-2 anti-spike polyclonal antibody raised in rabbit (P1R) and mice (MSer)
205 (obtained from BEI resources USA) were analysed for cross-reactivity with DENV. Using
206 confocal microscopy, we observed that both showed a significant cross-reactivity with an
207 average (MFI) of 13·2 for P1R and 13·4 for MSer (Fig. 5A-B). Mouse Monoclonal antibodies
208 against SARS-CoV-2, 1A9 (MFI of 7.4) and MM41 (MFI of 1.57), also showed cross-
209 reactivity with DENV-2. The positive-control, 4G2 (pan-flavivirus-anti-envelope antibody),
210 showed MFI of 18·28 whereas the Negative-control, anti-Rabies monoclonal (Rabishield®),
211 showed no reactivity with DENV-2. The binding kinetics of 1A9 (SARS-CoV-2 spike
212 antibody) showed a high affinity to DENV-2 Envelope with a dissociation constant (KD) of
213 4·84 μM (Fig. 5C ii-iii) using Bio-Layer Interferometry (BLI).

214

215 **SARS-CoV-2 spike antibodies enhance DENV infection**

216 Since DENV is endemic to India pre-existing anti-DENV antibodies may be responsible for the
217 observed ADE. To rule out this possibility, we further tested commercially available
218 monoclonal and polyclonal antibodies and sera raised in-house against the SARS-CoV-2 spike
219 and RBD for their potential to enhance the DENV-2 infection (Table-S6). All of the tested
220 antibodies (M1B, 1A9, MM41, P1R, M4B, M5B, Hser) enhanced DENV-2 infection (Fig. 6).
221 The RBD specific antibody (M5B) showed stronger enhancement compared to the antibody
222 against spike (MM41) with a dose-dependent increase in DENV-2 infection (Fig. 6A-B).
223 Similarly, hamster serum against purified SARS-CoV-2 spike protein also showed ADE of
224 DENV infection in K562 cells (Fig. 6C). Monoclonal antibody against Rabies virus (Negative-
225 control), did not show any ADE of dengue infection in K562 cells (Fig. 6C). A similar ADE
226 of DENV infection was observed in U937 cells too (Fig. S9). Three monoclonal antibodies –

227 4G2, 1A9, and M4B, showed significant ADE, as determined by the infectious titer of the virus
228 released in the culture supernatant from K562 cells (p-value<0·0001; Fig. S10).
229 Having established that there is an enhancement of DENV-2 infection due to anti-SARS-CoV-
230 2 antibodies, we next investigated whether it is time-dependent. We assessed ADE at 6 h, 18 h
231 and 36 h post-infection (Fig. S8). Mice (Mser) and hamster (Hser) sera, showed significant
232 ADE with respect to virus control (adjusted p-values Mser=0·0071 and Hser=0·0001), even at
233 6 hpi (Fig. S8). Although, we didn't observe a significant enhancement due to 4G2 and anti-
234 Spike monoclonals M3S and M2G at 6 hpi. At 18 hpi, a significant increase in the DENV-2
235 positive cells with respect to virus control was observed in 4G2 as well as M2G (Adjusted p-
236 value=0·0101), which further enhanced significantly at 36 hpi (Adjusted p-values 4G2=0·0001
237 and M2G=0·0035). The ADE in Hser reached saturation as early as 6 h (Adjusted p-
238 value<0·0001).
239
240 **Discussion:**
241 In this study, we demonstrate that SARS-CoV-2 antibodies cross-react with DENV-2 and
242 enhance DENV infection. Our work supports the work published by others highlighting SARS-
243 CoV-2 cross-reactivity and false positivity with dengue serology (21) (22). We used the DENV-
244 2E protein for BLI and computational studies since it has been reported to have maximum cross-
245 reactivity with SARS-CoV-2 S1 specific antibodies (12). A thorough *in silico* studies indicating
246 the high likeliness of cross-reactivity of SARS-CoV-2 spike antibodies with DENV-2.
247 Additionally, spike protein is critical for viral entry into cells and is the major target not only
248 for neutralizing antibodies but also for infection-enhancing antibodies (23). The dimeric
249 DENV-2 E-protein was used for docking studies, since we have intended to study the
250 interaction of DENV-2 with SARS-CoV-2 spike antibodies, which would happen before the

251 viral entry, extracellularly and it's known that the E-protein exists as a head-to-tail oriented
252 homodimer on the surface of mature-virions (24).
253 The *in-silico* results indicated that there is a significant interaction of SARS-CoV-2 antibodies
254 with DENV-2 dimeric E-protein. The binding free energy of SARS-CoV-2 antibodies i.e
255 CR3022 (6W7Y), S2E12 ab (7K45) and DMAb2196 (8D8R), being comparable to the DENV-
256 2 dimer specific antibody, C8 (4UTA). These top three binders shared their interacting interface
257 with C8 antibody. The residues involved in the interaction of C8 antibody with DENV-2 E were
258 also involved in the interaction of at-least one of the top three binders with E-protein (R73, E84,
259 R99, G102 and E311). The contributing residues which were found to be majorly stabilizing
260 the interaction of these top three SARS-CoV-2 antibodies with E-protein were S72, R73, Q77,
261 S81, N83 and R99 (involved in interacting epitopes of at least two out of the three). All the
262 residues involved in the interaction of these three SARS-CoV-2 antibodies with E-protein when
263 mapped, were majorly found to lie in the Domain-II and fusion-loop of E-protein. It is well
264 known that the antibodies against two epitopes of DENV are strong mediators of ADE: prM
265 epitopes (25) and fusion loop epitopes (26)**.** The fusion loop epitopes could be the ones,
266 potentially involved in ADE. Multiple residues have been identified from *in-silico* interaction
267 mining, among them few residues such as R73 (common among all), T70, S72 (Domain-II),
268 R99 and N103 (Fusion loop) and E311 (Domain-III) seem critical. These residues put forth the
269 possible avenue to explore further for epitope-based therapeutic interventions. The BLI findings
270 between dengue envelope protein and antibodies against SARS-CoV-2 spike protein indicate a
271 strong interaction with KD values in μM range.
272 We further assessed whether the SARS-CoV-2 antibodies could enhance DENV-2 infection *in-*
273 *vitro.* We found that convalescent plasma samples of SARS-CoV-2 recovered individuals,
274 collected at three different time intervals during COVID 19 pandemic, significantly enhanced
275 the DENV-2 infection in cultured Fc-receptor positive K562 and U937 cells. We also tested the

276 commercially available SARS-CoV-2 antibodies and Spike-immunized mice and hamster sera.
277 They showed an increased DENV-2 infection in both cell-based model.
278 The animal data observed strongly supported our *in-silco* and *in-vitro* data which clearly
279 showed that SARS-CoV-2 spike antibodies mediated enhancement of dengue virus infection.
280 However, the platelet counts and hematocrit levels were not significantly affected. Also, the
281 increased viral load as indicated by FFU and viral RNA levels in spleen and liver (Fig. 4d, e, f)
282 did not translate to increase the disease severity. However, the increased viral load might be
283 enhancing the clinical symptoms, which could be one reason for increased symptomatic cases
284 reported during late pandemic. Still, the surge of dengue cases was not observed during the
285 early stages of pandemic, which might be due to underreporting or reduced testing for dengue
286 during the peak COVID-19 pandemic as the clinical symptoms of both viruses are very similar.
287 Our study doesn't provide the mechanistic insights into the pathway involved in ADE of
288 DENV-2 infection due to SARS-CoV-2 antibodies. The extrinsic pathway, involves an
289 enhanced FcR-mediated entry of the virus into the host cells leading to an increase in the
290 number of infected cells, whereas the intrinsic pathway, involves a suppression of the host
291 antiviral immune response causing increased viral replication and would boost virus production
292 per infected cell (27) (28). Here we briefly did a time-course based study of DENV-2 infection
293 upon treatment of virus with SARS-CoV-2 antibodies and convalescent plasma. We observed
294 an enhancement in the percentage of DENV-2 infected cells, even at 6 h, indicating enhanced
295 virus internalization, since this is before E-protein from replicated new virions is expected (23)
296 (24) which may possibly indicate the presence of at least extrinsic pathway for ADE. However,
297 it needs further exploration for confirmation.
298 The DENV-2 used for the in-vitro assay was prepared in C6/36 cells and wasn't characterized
299 for the proportions of immature and mature-virions. It is well known that the virus prepared *in-*
300 *vitro* in mosquito cells has a considerably greater number of immature virions as compared to

301 mammalian cells, probably due to differential furin-expression (29) (30). Also, it is recognized
302 that laboratory adapted DENV strains are more dynamic than clinical strains and expose cryptic
303 epitopes more easily (31). Thus our virus preparation might have major proportion of immature
304 virions but this probably won't change the fact that the ADE of DENV-infection would happen
305 since the viral heterogeneity in response to the natural DENV-infections is also well known
306 The antibody repertoire in the natural infections is known to have an abundance of poorly
307 neutralizing antibodies which are majorly generated in response to the immature conformations
308 (32), which is a result of incomplete furin processing, resulting in egress of immature-forms
309 along with and mature-forms of virions post-assembly (33) (34). Also, the fully mature-virions
310 have been reported to be less susceptible to neutralization by cross-reactive and heterotypic
311 immune sera than partially mature variants (32)**.** Thus, the heterogeneity in the DENV-2
312 preparation used for the *in-vitro* assays can be probably closely related to the natural infection
313 scenario. Further, our results from the BLI and docking studies are based on the dimeric form
314 of E-protein (indicating mature-form). Thus, one may then ask that the cross-reactive epitopes
315 defined here, might not be all the interacting epitopes that would possibly be involved and
316 interactions with other conformations must also be considered. Although it can be challenging
317 to map the exact cross-reactive epitopes since DENV is known to have multiple transient states,
318 involving different arrangements and oligomeric states of E-proteins that which governs the
319 antigenic landscape or accessibility of DENV (35). Still, a docking study with a heterotrimer of
320 E-protein (consisting of un-cleaved prM), being a crystallized transient state (36) may give a
321 better indication of more of the cross-reactive epitopes involved.
322 It would be informative to investigate if the antibodies induced in response to various SARS-
323 CoV-2 vaccines also possess the potential to enhance DENV-infection. Since a recent study by
324 Kaur *et. al.,* in North India revealed a twofold higher risk of symptomatic dengue in individuals
325 with a history of COVID-19 in 2020. Additionally, those who received the COVID-19 vaccine

326 after recovering from COVID-19 showed a 3.6 times higher likelihood of developing
327 symptomatic dengue compared to individuals without a history of COVID-19 or vaccination
328 (11). These findings have significant implications keeping in view the co-circulation of both
329 DENV-2 and SARS-CoV-2 in several countries and thus the vaccine development strategies
330 against both the agents might need an inevitable change.

331 **Materials and Methods:**

332 **Molecular docking of DENV-2 Envelope glycoprotein and SARS- CoV-2 antibodies:**

333 **Curation of data:**

334 X-ray crystal structures of DENV-2 envelope glycoprotein (PDB ID:4UT6) (37) and SARS-
335 CoV-2 antibodies were curated from RCSB in PDB format (http://www.rcsb.org/pdb). These
336 crystal structures along with their corresponding resolution values, and are summarized in –
337 Table-S1. Crystal structure of antibodies were curated by removal of spike protein, water
338 molecules and metal ions using UCSF Chimera 1·15 (38). All structures were prepared using
339 Maestro's Protein Preparation Wizard module (Schrödinger Release 2020-1) (39). The
340 hydrogens and bond orders were added, missing side-chains and loops were filled by Prime
341 (39). The hydrogen bond (HB) optimization and restrained minimizations were also done for
342 the systems using force field OPLS4 (40).

343 **Protein-Antibody docking and choosing the best pose:**

344 Protein-protein interactions govern various aspects of structural and functional cellular
345 mechanisms, and their elucidation is crucial for a better understanding of biological processes.
346 All the prepared SARS-CoV-2 antibodies, along with controls i.e positive (pdb-id:4UTA) and
347 negative control (pdb-id:7U9G) were docked on prepared DENV2 E protein structure by

348 masking non-CDR regions of antibodies. The Chothia definition is used for the CDR region.
349 Multiple docking methods were used to minimize the biases by including HDOCK (41),
350 pyDock (42) and Piper program (43). The rationale for implementing multiple docking
351 programs was to obtain the consensus results from all three tools and to remove any false-
352 positive outcomes. Best poses were chosen from docked models on the basis of their docking
353 score, cluster size (44) and reported paratope residues (45) (46) (47).

354 **Thermodynamic quantification using Molecular Mechanics-Generalized Born Surface**
355 **Area (MM-GBSA):**

356 The binding free energy of protein and antibody complexes was carried out in Prime MM-
357 GBSA (Molecular Mechanics Generalized Born Surface Area) by Prime (48) module of
358 Schrodinger suite. We used the VSGB solvation model and OPLS4 force field. The binding
359 free energy is calculated by: MMGBSA dG Bind (NS) = Complex – Receptor (from optimized
360 complex) – Ligand (from optimized complex) = MMGBSA dG Bind–Rec Strain–Lig Strain,
361 Where, Rec Strain = Receptor (from optimized complex) – Receptor, Lig Strain = Ligand (from
362 optimized complex) – Ligand, MMGBSA dG Bind = Complex – Receptor – Ligand, NS = no
363 strain.

364 **Figures:**

365 All figures were generated using VMD (V.1·9·1) (49) and graphs were generated using the
366 XMGRACE (Version 5·1·19) (47).

367 **Cells:**

368 Human myeloid cell lines K562 (ATCC CCL-243) and U937 (ATCC CRL-1593.2) were
369 cultured in Iscove's Modified Dulbecco's media (IMDM, HIMEDIA) and Roswell Park

370 Memorial Institute (RPMI, Gibco) 1640 respectively. African Green Monkey cell line Vero E6
371 (NCCS, India) was maintained in Dulbecco's Modified Eagle Medium (DMEM, HIMEDIA)
372 while A. albopictus cell line C6/36 (NCCS, India) was cultivated in Leibovitz's L-15 Medium
373 (HIMEDIA). All the cells were maintained in respective media supplemented with 100 U/ml
374 of penicillin, 100 μg/ml of streptomycin (HIMEDIA), and 10% Fetal Bovine Serum
375 (HIMEDIA). C6/36 cells were maintained at 28°C (ESCO incubator) without CO_2 while the
376 other cells were grown in a humidified 37°C incubator (Thermo Fisher Scientific) with 5%
377 CO_2.

378 **Virus stocks:**

379 Dengue virus serotype 2 (NGC strain) was propagated in C6/36 cells and it was used for all the
380 assays. The cells at a confluency of 60-70% were infected with Dengue virus at a multiplicity
381 of infection (MOI) of 0·1 using inoculum prepared in L-15 medium supplemented with 2%
382 FBS. It was incubated with cells for 2 h at 28°C with intermittent rocking. Subsequently, the
383 cells were washed and incubated with L-15 medium with 10% FBS. Culture supernatant was
384 harvested at 5 dpi, clarified by centrifugation at 129 ×*g* at room temperature and concentrated
385 using centrifugal ultrafiltration (Amicon® Ultra centrifugal filter (100 kDa), ACS510024 from
386 Millipore, Darmstadt, Germany) at 3220 ×*g* for 10 min for every 15 ml of supernatant. The
387 infectious titer of the virus was determined by a focus-forming unit (FFU) assay performed in
388 Vero E6 cells.

389 The three variants of SARS-CoV-2, original Wuhan (USA-WA1/2020, Genbank: MN985325),
390 B·1·617·2 (δ-variant) known as THSTI_287 (GenBank: MZ356566·1), and Omicron
391 BA·1(GISAID accession no.: EPI_ISL_8764350) were propagated in Vero E6 cells. Cells were
392 infected with 0·1 MOI of virus inoculum and incubated for 1 h with shaking at 37°C. Virus
393 supernatant was harvested at 48 hpi, filtered, and stored at -80°C. The infective titer was

394 determined by titration on Vero E6 cells using the $TCID_{50}$ method (50). These virus stocks were
395 used for neutralization assays.

396 **Serum samples and Antibodies:**

397 We selected a group of convalescent plasma samples (n=48) collected at three different time
398 intervals during COVID-19 pandemic in India. They are defined as follows: the first interval
399 was from May 2020 to January 2021, second interval from May 2021 to June 2021, third
400 interval from February 2022 to April 2022. The clinical details of the samples are given in the
401 Table S1. The pan flavivirus, anti-envelope mAb, 4G2 was purified inhouse from HB112
402 hybridoma cells. SARS-CoV-2 spike (S2 specific) antibody 1A9 was purchased from Gentex
403 while Anti- Recombinant SARS-CoV-2 Spike Protein (whole spike) Sino 4059-MM41 was
404 purchased from Sino Biologicals. Other SARS CoV2-related antibodies M1B, M4B, M5B, P1R
405 were obtained from BEI resources, USA. SARS CoV2 infected mice and hamster serum were
406 generated inhouse. Rabies Human monoclonal antibody, Rabishield®-100 (Serum Institute of
407 India), was purchased from the pharmacy. All the details regarding commercial antibodies/
408 serum are mentioned in - Table S2.

409 **Confocal microscopy:**

410 0.5 x 10^6 C6/36 cells from an exponentially growing culture were seeded on grass cover slips
411 followed by DENV-2 at 1.0 MOI. At 48 h post-infection the cells were fixed with 3.7%
412 paraformaldehyde (PFA) and permeabilized using 0.1% Triton-X-100. The cells were immune-
413 stained with primary antibody and fluor-conjugated secondary antibodies. Subsequently,
414 coverslips were mounted onto glass slides using ProLong Gold Antifade Mountant
415 supplemented with DAPI. Fluorescence was observed under 60X magnification using a
416 FLUOVIEW FV3000 confocal microscope (Olympus). The mean fluorescence intensity (MFI)

417 was calculated using images from 10 fields per slide with 7 cells per field (at least 70 data
418 points). Statistical analysis employed One-way ANOVA followed by Dunnett's test, comparing
419 to the negative control (Rabishield).

420 **Live Virus Neutralization Assay:**

421 Two-fold serial dilutions of heat-inactivated plasma samples were mixed with 100 $TCID_{50}$ of
422 SARS-CoV-2 virus and subsequently allowed to infect Vero E6 monolayers. After incubation
423 for 72 h at 37°C with 5% CO_2, the degree of CPE was qualitatively determined under a
424 microscope. Absence of CPE indicated virus neutralization, and the highest dilution that
425 completely prevented emergence of CPE was considered as the neutralization titer. For plasma
426 samples collected during-the third interval, cells were fixed 24 h post-infection and immune-
427 stained using antibody against the SARS-CoV-2 Nucleocapsid protein (1:2000, 4H2,
428 Genscript), followed by Alexa 488 conjugated anti-mouse antibody (1:500, Invitrogen).
429 Fluorescent foci were quantified by AID iSpot Reader with AID EliSpot 8.0 iSpot software.

430 **Antibody-dependent Enhancement (ADE) Assay:**

431 Serum samples (15 µl) and commercial antibodies (5 µl) were diluted in plain Iscove's Modified
432 Dulbecco's Medium (IMDM) to a total volume of 100 µl. Subsequently, 100 µl of virus dilution
433 was added, and the mixture was incubated at 37°C for 1 h. The virus-antibody complexes were
434 then allowed to infect 1 x 10^6 cells K562/U937 cells for 2 h at an MOI 1. After infection the
435 cells were washed and incubated in IMDM-2% FBS at 37°C, 5% CO_2 for 36 h. Subsequently,
436 cells were fixed using 4% PFA, permeabilized with 0.1% Triton X-100, immune-stained with
437 purified 4G2 (dilution 1:200), and Alexa-Fluor 488 conjugated anti-mouse (dilution 1:500).
438 The number of cells positive for DENV antigen was quantified by flow cytometry.

439 **Flow Cytometry Analysis:**

440 Flow cytometry was conducted using a BD FACS Canto II flow cytometer (BD Biosciences)
441 with 20,000 cells acquired per sample through FACS Diva software. FlowJo v10.8.1 was used
442 for analysis. Live cells were gated based on FSC and SSC, followed by singlet determination
443 using FSC-A vs FSC-H gate. Dengue virus-positive cells were gated on the FITC channel using
444 singlet population. FITC voltage was set using isotype control. Fcγ receptor expression was
445 assessed with anti-CD64 (Alexa Fluor 700), anti-CD32 (PE), and anti-CD16 (APC) antibodies
446 in K562 and U937 cells. Statistical analysis was conducted in GraphPad Prism 8.

447 **Detection of DENV RNA using Quantitative RT-PCR:**

448 Total RNA from 1 x 10^6 K562 cells was extracted using the standard TRIzol method. RNA was
449 quantitated using Nanodrop (Thermofisher Scientific) and 300 ng RNA was used for qPCR
450 using a one-step RT-PCR kit (SOLIScript® 1-step Probe kit, Solis Biodyne) following the
451 manufacturer's protocol for detection of DENV2 RNA. GAPDH was used as an internal
452 control. Fold change in DENV2 RNA copies was calculated with respect to GAPDH. The
453 details regarding primer and probe sequences are given in - Table S7.

454 **Binding kinetics using Biolayer Interferometry (BLI):**

455 BLI studies were performed on an Octet RED 96 instrument at 24°C with shaking at 1000 rpm
456 (ForteBIO). For DENV-2 Envelope protein, the buffer composition was 50mM Tris, 150mM
457 NaCl, 0.5% glycerol, pH 8.0. Whereas, for SARS-CoV-2 Spike protein, phosphate buffered
458 saline, pH 7.4 was used. Sensors were in the respective kinetic buffer (51). For studying binding
459 kinetics with protein E, antibodies at a concentration of 5 µg/ml were loaded onto the sensors
460 (AHC (Anti-hIgG Fc Capture) for CR3022 and C8, protein G (for 1A9 antibody)) DENV E
461 dimeric protein was diluted serially three-fold (starting with 6000nM) and Spike trimeric
462 protein was diluted 2 fold (starting with 600nM) in their respective kinetic buffers. The

designed experiment started with a baseline (100Sec), followed by 3 cycles of neutralization and regeneration and again a baseline (100Sec). After this step, antibody loading was performed (700sec) onto all the 5 sensors. After the loading step, another baseline (baseline2, 60sec), Association was performed after the 2nd baseline step for 300sec, followed by 300sec dissociation.

Here the 5th sensor was used as reference where no analyte was used, where the analyte concentration was kept 0nM. The same sensor during the data processing was assigned as reference well (change well type-reference well) and same wells; reference well, were subtracted from the raw data. Here the ligand and analyte dilution as well as the whole experiment was performed in the respective kinetic buffers. The binding responses were calculated and fitting globally with a 1:1 binding model using ForteBio's Data Analysis software 10·1. The data was considered validated if $X^2 < 0{\cdot}5$.

Mouse Infection

The AG129 (IFNα/β/γR -/- 129/Sv) mice were obtained from the Jackson laboratory, USA and maintained in small animal facility (SAF), RCB, Faridabad, India. All experiments with AG129 mice were performed in 6-8 weeks old mice of either sex. One group of mice were treated (one-time through intranasal route) with human ACE2 adenovirus using 2.5×10^8 PFU for transient expression of hACE2 in lungs and respiratory track. After five days mice were infected with SARS CoV-2 via nasal route inoculation using 1×10^5 PFU virus. Mice were bled at day7, 14 and 21 post SARS CoV-2 infection to measure the antibodies against SARS CoV-2. At day 21 both the groups were challenged with 1×10^4 FFU mouse-adapted DENV2 (P8-P23085 INDI-60) and were euthanized on the moribund state.

Focus forming unit (FFU) assay

486 FFU assay was carried out to determine the virus titer in the serum of DENV2 infected
487 AG129 mice with slight modifications. Vero E6 cells were seeded at a density of $0.01x10^6$
488 cells/well in a 96-well black/clear bottom plate and cells were allowed to reach 80%
489 confluency. At 80% confluency 100 µl of 10-fold serially diluted serum in media with 2%
490 FBS was added to the wells and incubated. After 2 hr, serum was removed, fresh media with
491 2% FBS was added and incubated for 24 hr at 37° C in 5% CO_2. Following that cells were
492 fixed with 2% PFA and the immunostaining for virus detection was performed using mAb
493 4G2 (pan-DENV anti-envelope antibody), followed by secondary antibody, goat anti-mouse
494 IgG, AF488 conjugated (Invitrogen) prepared in permeabilization buffer (0.1% triton x100
495 with 2%BSA in PBS). The foci were visualized and counted using fluorescence microscope.

496 **Quantitative real time PCR**

497 Total RNA from the mice tissues was extracted using RNAiso (Takara Bio, Japan) followed by
498 phenol-chloroform treatment. The first strand cDNA was synthesized from 1µg RNA using
499 cDNA synthesis kit (BioRad, USA) as per manufacturer's protocol. The cDNA was used for
500 real-time PCR using SYBR green supermix (BioRad) in an Applied Biosystems Quant
501 Studio™ 6 Flex Real-Time PCR System. The primers set used for detection of the respective
502 genes are given in Table S8.

503 **Statistical analysis:**

504 Experimental values were represented as mean ± standard deviation (SD). Statistical analysis
505 was done using the ordinary one-way ANOVA followed by Dunnett's multiple comparison
506 test, using GraphPad Prism version 8·4·2. Differences were considered significant at p-value <
507 0·05.
508

Acknowledgements:

The following reagent was obtained through BEI Resources, NIAID, NIH: SARS-Related Coronavirus 2, Isolate USA-WA1/2020, NR-52281, Monoclonal Anti-SARS-Related Coronavirus 2 Spike Glycoprotein, Clone 1-3D7 (produced *in-vitro*), NR-56488, Monoclonal Anti-SARS-Related Coronavirus 2 Spike Glycoprotein Receptor Binding Domain-(RBD), Clone 2TP1C3 (produced *in-vitro*), NR-55296, Polyclonal Anti-SARS-Related Coronavirus 2 Spike Glycoprotein (IgG, Rabbit), NR-52947." The RBD is proprietary reagents with IP No. 202011018845, we thank Dr. Barney Graham (VRC/NIAID/NIH) for providing us with spike construct (SARS-2-CoV S 2P). We would like to thank Prof. Shinjini Bhatnagar, Prof. Pramod Garg and Prof. Jayanta Bhattacharya from THSTI for critically reviewing the manuscript, ABSL3 facility committee and staff for their help and support. This research has been conducted with the significant contribution and expertise of THSTI, NCR Biotech Science Cluster BIOREPOSITORY and DBT India Consortium".

DBT India Consortium**, ** Name of all the collaborating Institutes/ Hospitals: Translational Health Science Technology Institute, Clinical partners: Maulana Azad Medical College, Lok Nayak Jai Prakash Hospital, and Lady Hardinge Medical College in Delhi, ESI Medical College Hospital, Faridabad, Civil Hospital, Gurugram, Haryana; Civil Hospital, Palwal, Haryana; Al-Falah School of Medical Science & Research Centre and Hospital, Dhauj, Haryana; Medanta Hospital, Gurugram; Shaheed Hasan Khan Mewati Government Medical College, Nalhar, Haryana.

Data availability:

All the data are presented in this manuscript. The virus strains used in this study have the following accession numbers: original Wuhan (USA-WA1/2020, Genbank: MN985325),

533 B·1·617·2 (δ-variant) known as THSTI_287 (GenBank: MZ356566·1), and Omicron BA·1
534 (GISAID accession no.: EPI_ISL_8764350) Source data are provided with this paper.
535
536 **Author Contributions:**
537 SM conceptualized the idea. SM, SB, SA, TrS and PG coordinated the research activity. KJ
538 and SS contributed to designing and execution of viral assays. KJ, SS, GS, NB, TS, MT, JK,
539 DKR, BL, SK, PS, SK, VP, S, LK and VG contributed to data curation, investigation and
540 methodology. KJ, SS, TRA, GJ, GS, SB, SA, TrS, PG and SM contributed to formal analysis.
541 SS, SR, MG, PK, NW, RT, SB, TrS, SA and SM provided resources. KJ, SS, TRA, GJ, TrS,
542 PK, NW, RT, SB, SA, PG and SM contributed to writing, review & editing the draft. All authors
543 had full access to all the data in the study and had final responsibility for the decision to submit
544 for publication.
545
546 **Ethics statement**
547 We obtained the approval from the Institutional Bio-Safety Committee prior to conducting the
548 studies: (IBSC#495/2023), RCGM (No.-BT/IBKP/137/2020), RCGM (No.BT/IBKP/053/
549 2020).
550
551 **Disclosure statement**
552 The Author declares no conflict of interest.
553
554 **Funding:**
555 The current research is funded by the Translational Research Program Grant,
556 BT/PR30159/MED/15/188/2018, THSTI Core and the Bill and Melinda Gates Foundation
557 GIISER-South Asia (INV-030592). The computational work was supported by the national

network project (NNP-BT/PR40189/BTIS/137/50/2022), DBT. The work on dengue envelope proteins was done with support of funding received from NBM (National Biopharma Mission) scheme of BIRAC (Biotechnology Industry Research Assistance Council), India (BT/NBM099/02/18) (2019-2023). SK acknowledge NBM BIRAC for his fellowship support.

564 **Reference:**

565

566 1. WHO. WHO, Fact sheets / Detail / Dengue and severe dengue 2023 [cited 2023 11th
567 December]. Available from: https://www.who.int/news-room/fact-sheets/detail/dengue-
568 and-severe-dengue.
569 2. Lee MF, Voon GZ, Lim HX, Chua ML, Poh CL. Innate and adaptive immune evasion by
570 dengue virus. Front Cell Infect Microbiol. 2022;12:1004608. Epub 2022/10/04. doi:
571 10.3389/fcimb.2022.1004608. PubMed PMID: 36189361; PubMed Central PMCID:
572 PMCPMC9523788.
573 3. Pierson TC, Diamond MS. A game of numbers: the stoichiometry of antibody-
574 mediated neutralization of flavivirus infection. Prog Mol Biol Transl Sci. 2015;129:141-66.
575 Epub 2015/01/18. doi: 10.1016/bs.pmbts.2014.10.005. PubMed PMID: 25595803; PubMed
576 Central PMCID: PMCPMC4910618.
577 4. Khan S, Akbar SMF, Yahiro T, Mahtab MA, Kimitsuki K, Hashimoto T, et al. Dengue
578 Infections during COVID-19 Period: Reflection of Reality or Elusive Data Due to Effect of
579 Pandemic. Int J Environ Res Public Health. 2022;19(17). Epub 2022/09/10. doi:
580 10.3390/ijerph191710768. PubMed PMID: 36078486; PubMed Central PMCID:
581 PMCPMC9518125.
582 5. Khan S, Akbar SMF, Nishizono A. Co-existence of a pandemic (SARS-CoV-2) and an
583 epidemic (Dengue virus) at some focal points in Southeast Asia: Pathogenic importance,
584 preparedness, and strategy of tackling. Lancet Reg Health Southeast Asia. 2022;4:100046.
585 Epub 2022/07/26. doi: 10.1016/j.lansea.2022.100046. PubMed PMID: 35873345; PubMed
586 Central PMCID: PMCPMC9296506 interest.
587 6. Lu X, Bambrick H, Pongsumpun P, Dhewantara PW, Toan DTT, Hu W. Dengue
588 outbreaks in the COVID-19 era: Alarm raised for Asia. PLoS Negl Trop Dis.
589 2021;15(10):e0009778. Epub 2021/10/09. doi: 10.1371/journal.pntd.0009778. PubMed
590 PMID: 34624031; PubMed Central PMCID: PMCPMC8500420.
591 7. Manna S, Satapathy P, Bora I, Padhi BK. Dengue outbreaks in South Asia amid Covid-
592 19: Epidemiology, transmission, and mitigation strategies. Front Public Health.
593 2022;10:1060043. Epub 2023/01/03. doi: 10.3389/fpubh.2022.1060043. PubMed PMID:
594 36589966; PubMed Central PMCID: PMCPMC9797821.
595 8. Oladipo HJ, Rabiu I, Tajudeen YA. Dengue virus and SARS-CoV-2 Co-infection
596 dynamics: An emerging threat among African countries. Ann Med Surg (Lond).
597 2022;82:104398. Epub 2022/08/30. doi: 10.1016/j.amsu.2022.104398. PubMed PMID:
598 36035770; PubMed Central PMCID: PMCPMC9394095.
599 9. Prapty C, Rahmat R, Araf Y, Shounak SK, Noor AA, Rahaman TI, et al. SARS-CoV-2 and
600 dengue virus co-infection: Epidemiology, pathogenesis, diagnosis, treatment, and
601 management. Rev Med Virol. 2023;33(1):e2340. Epub 2022/03/04. doi: 10.1002/rmv.2340.
602 PubMed PMID: 35238422; PubMed Central PMCID: PMCPMC9111128.
603 10. Rana MS, Usman M, Alam MM, Ikram A, Salman M, Umair M. Impact of previous
604 SARS-CoV-2 infection on the rate of mortality in dengue. A preliminary report from Pakistan.
605 J Infect. 2022;84(5):722-46. Epub 2022/01/27. doi: 10.1016/j.jinf.2022.01.027. PubMed
606 PMID: 35081438; PubMed Central PMCID: PMCPMC8783977 of interest.
607 11. Kaur U, Jethwani P, Mishra S, Dehade A, Yadav AK, Chakrabarti S, et al. Did COVID-19
608 or COVID-19 Vaccines Influence the Patterns of Dengue in 2021? An Exploratory Analysis of

609 Two Observational Studies from North India. Am J Trop Med Hyg. 2023;109(6):1290-7. Epub
610 2023/10/31. doi: 10.4269/ajtmh.23-0418. PubMed PMID: 37903443.
611 12. Masyeni S, Santoso MS, Widyaningsih PD, Asmara DW, Nainu F, Harapan H, et al.
612 Serological cross-reaction and coinfection of dengue and COVID-19 in Asia: Experience from
613 Indonesia. Int J Infect Dis. 2021;102:152-4. Epub 2020/10/30. doi:
614 10.1016/j.ijid.2020.10.043. PubMed PMID: 33115680; PubMed Central PMCID:
615 PMCPMC7585717.
616 13. Alla D, Alla SSM, Vempati R, Bhatt H, Sultana Q, Bhatt S, et al. Dengue & COVID-19: A
617 Comparison and the Challenges at Hand. Cureus. 2022;14(11):e31877. Epub 2022/12/30.
618 doi: 10.7759/cureus.31877. PubMed PMID: 36579259; PubMed Central PMCID:
619 PMCPMC9792364.
620 14. Digwo DC, Elebe CP, Chigor VN, Madueke SN, Ezeh CK, Ike AC. Occurrence of False-
621 Positive Tests and Cross-reactions Between COVID-19 and Dengue With Implications During
622 Diagnosis: A Mixed Evidence Synthesis. Infectious Microbes & Diseases. 2023;5(2):64-75. doi:
623 10.1097/im9.0000000000000116. PubMed PMID: 02123149-202306000-00004.
624 15. Ulrich H, Pillat MM, Tarnok A. Dengue Fever, COVID-19 (SARS-CoV-2), and Antibody-
625 Dependent Enhancement (ADE): A Perspective. Cytometry A. 2020;97(7):662-7. Epub
626 2020/06/09. doi: 10.1002/cyto.a.24047. PubMed PMID: 32506725; PubMed Central PMCID:
627 PMCPMC7300451.
628 16. Cheng YL, Chao CH, Lai YC, Hsieh KH, Wang JR, Wan SW, et al. Antibodies against the
629 SARS-CoV-2 S1-RBD cross-react with dengue virus and hinder dengue pathogenesis. Front
630 Immunol. 2022;13:941923. Epub 2022/09/02. doi: 10.3389/fimmu.2022.941923. PubMed
631 PMID: 36045680; PubMed Central PMCID: PMCPMC9420930.
632 17. Nath H, Mallick A, Roy S, Kayal T, Ranjan S, Sengupta S, et al. COVID-19 serum can be
633 cross-reactive and neutralizing against the dengue virus, as observed by the dengue virus
634 neutralization test. Int J Infect Dis. 2022;122:576-84. Epub 2022/07/11. doi:
635 10.1016/j.ijid.2022.07.013. PubMed PMID: 35811081; PubMed Central PMCID:
636 PMCPMC9262656.
637 18. El-Qushayri AE, Kamel AMA, Reda A, Ghozy S. Does dengue and COVID-19 co-
638 infection have worse outcomes? A systematic review of current evidence. Rev Med Virol.
639 2022;32(5):e2339. Epub 2022/02/26. doi: 10.1002/rmv.2339. PubMed PMID: 35213764;
640 PubMed Central PMCID: PMCPMC9111070.
641 19. Srivastava M, Suri C, Singh M, Mathur R, Asthana S. Molecular dynamics simulation
642 reveals the possible druggable hot-spots of USP7. Oncotarget. 2018;9(76):34289-305. Epub
643 2018/10/23. doi: 10.18632/oncotarget.26136. PubMed PMID: 30344943; PubMed Central
644 PMCID: PMCPMC6188144.
645 20. Littaua R, Kurane I, Ennis FA. Human IgG Fc receptor II mediates antibody-dependent
646 enhancement of dengue virus infection. J Immunol. 1990;144(8):3183-6. Epub 1990/04/15.
647 PubMed PMID: 2139079.
648 21. Yan G, Lee CK, Lam LTM, Yan B, Chua YX, Lim AYN, et al. Covert COVID-19 and false-
649 positive dengue serology in Singapore. Lancet Infect Dis. 2020;20(5):536. Epub 2020/03/08.
650 doi: 10.1016/S1473-3099(20)30158-4. PubMed PMID: 32145189; PubMed Central PMCID:
651 PMCPMC7128937.
652 22. Lustig Y, Keler S, Kolodny R, Ben-Tal N, Atias-Varon D, Shlush E, et al. Potential
653 Antigenic Cross-reactivity Between Severe Acute Respiratory Syndrome Coronavirus 2 (SARS-
654 CoV-2) and Dengue Viruses. Clin Infect Dis. 2021;73(7):e2444-e9. Epub 2020/08/17. doi:

655 10.1093/cid/ciaa1207. PubMed PMID: 32797228; PubMed Central PMCID:
656 PMCPMC7454334.
657 23. Wahala WM, Silva AM. The human antibody response to dengue virus infection.
658 Viruses. 2011;3(12):2374-95. Epub 2012/02/23. doi: 10.3390/v3122374. PubMed PMID:
659 22355444; PubMed Central PMCID: PMCPMC3280510.
660 24. Modis Y, Ogata S, Clements D, Harrison SC. A ligand-binding pocket in the dengue
661 virus envelope glycoprotein. Proc Natl Acad Sci U S A. 2003;100(12):6986-91. Epub
662 2003/05/22. doi: 10.1073/pnas.0832193100. PubMed PMID: 12759475; PubMed Central
663 PMCID: PMCPMC165817.
664 25. Rodenhuis-Zybert IA, van der Schaar HM, da Silva Voorham JM, van der Ende-
665 Metselaar H, Lei HY, Wilschut J, et al. Immature dengue virus: a veiled pathogen? PLoS
666 Pathog. 2010;6(1):e1000718. Epub 2010/01/12. doi: 10.1371/journal.ppat.1000718.
667 PubMed PMID: 20062797; PubMed Central PMCID: PMCPMC2798752.
668 26. de Alwis R, Williams KL, Schmid MA, Lai CY, Patel B, Smith SA, et al. Dengue viruses
669 are enhanced by distinct populations of serotype cross-reactive antibodies in human
670 immune sera. PLoS Pathog. 2014;10(10):e1004386. Epub 2014/10/03. doi:
671 10.1371/journal.ppat.1004386. PubMed PMID: 25275316; PubMed Central PMCID:
672 PMCPMC4183589.
673 27. Modhiran N, Kalayanarooj S, Ubol S. Subversion of innate defenses by the interplay
674 between DENV and pre-existing enhancing antibodies: TLRs signaling collapse. PLoS Negl
675 Trop Dis. 2010;4(12):e924. Epub 2011/01/05. doi: 10.1371/journal.pntd.0000924. PubMed
676 PMID: 21200427; PubMed Central PMCID: PMCPMC3006139.
677 28. Ubol S, Phuklia W, Kalayanarooj S, Modhiran N. Mechanisms of immune evasion
678 induced by a complex of dengue virus and preexisting enhancing antibodies. J Infect Dis.
679 2010;201(6):923-35. Epub 2010/02/18. doi: 10.1086/651018. PubMed PMID: 20158392.
680 29. Murray JM, Aaskov JG, Wright PJ. Processing of the dengue virus type 2 proteins prM
681 and C-prM. J Gen Virol. 1993;74 (Pt 2):175-82. Epub 1993/02/01. doi: 10.1099/0022-1317-
682 74-2-175. PubMed PMID: 8429301.
683 30. Davis CW, Nguyen HY, Hanna SL, Sanchez MD, Doms RW, Pierson TC. West Nile virus
684 discriminates between DC-SIGN and DC-SIGNR for cellular attachment and infection. J Virol.
685 2006;80(3):1290-301. Epub 2006/01/18. doi: 10.1128/JVI.80.3.1290-1301.2006. PubMed
686 PMID: 16415006; PubMed Central PMCID: PMCPMC1346927.
687 31. Chaichana P, Okabayashi T, Puiprom O, Sasayama M, Sasaki T, Yamashita A, et al. Low
688 levels of antibody-dependent enhancement in vitro using viruses and plasma from dengue
689 patients. PLoS One. 2014;9(3):e92173. Epub 2014/03/20. doi:
690 10.1371/journal.pone.0092173. PubMed PMID: 24642752; PubMed Central PMCID:
691 PMCPMC3958444.
692 32. Beltramello M, Williams KL, Simmons CP, Macagno A, Simonelli L, Quyen NT, et al.
693 The human immune response to Dengue virus is dominated by highly cross-reactive
694 antibodies endowed with neutralizing and enhancing activity. Cell Host Microbe.
695 2010;8(3):271-83. Epub 2010/09/14. doi: 10.1016/j.chom.2010.08.007. PubMed PMID:
696 20833378; PubMed Central PMCID: PMCPMC3884547.
697 33. Pierson TC, Diamond MS. Degrees of maturity: the complex structure and biology of
698 flaviviruses. Curr Opin Virol. 2012;2(2):168-75. Epub 2012/03/27. doi:
699 10.1016/j.coviro.2012.02.011. PubMed PMID: 22445964; PubMed Central PMCID:
700 PMCPMC3715965.

701 34. Cherrier MV, Kaufmann B, Nybakken GE, Lok SM, Warren JT, Chen BR, et al.
702 Structural basis for the preferential recognition of immature flaviviruses by a fusion-loop
703 antibody. EMBO J. 2009;28(20):3269-76. Epub 2009/08/29. doi: 10.1038/emboj.2009.245.
704 PubMed PMID: 19713934; PubMed Central PMCID: PMCPMC2771083.
705 35. Holzmann H, Stiasny K, York H, Dorner F, Kunz C, Heinz FX. Tick-borne encephalitis
706 virus envelope protein E-specific monoclonal antibodies for the study of low pH-induced
707 conformational changes and immature virions. Arch Virol. 1995;140(2):213-21. Epub
708 1995/01/01. doi: 10.1007/BF01309857. PubMed PMID: 7535997.
709 36. Rey FA, Stiasny K, Vaney MC, Dellarole M, Heinz FX. The bright and the dark side of
710 human antibody responses to flaviviruses: lessons for vaccine design. EMBO Rep.
711 2018;19(2):206-24. Epub 2017/12/29. doi: 10.15252/embr.201745302. PubMed PMID:
712 29282215; PubMed Central PMCID: PMCPMC5797954.
713 37. Rouvinski A, Guardado-Calvo P, Barba-Spaeth G, Duquerroy S, Vaney MC, Kikuti CM,
714 et al. Recognition determinants of broadly neutralizing human antibodies against dengue
715 viruses. Nature. 2015;520(7545):109-13. Epub 2015/01/13. doi: 10.1038/nature14130.
716 PubMed PMID: 25581790.
717 38. Pettersen EF, Goddard TD, Huang CC, Couch GS, Greenblatt DM, Meng EC, et al. UCSF
718 Chimera--a visualization system for exploratory research and analysis. J Comput Chem.
719 2004;25(13):1605-12. Epub 2004/07/21. doi: 10.1002/jcc.20084. PubMed PMID: 15264254.
720 39. Sastry GM, Adzhigirey M, Day T, Annabhimoju R, Sherman W. Protein and ligand
721 preparation: parameters, protocols, and influence on virtual screening enrichments. J
722 Comput Aided Mol Des. 2013;27(3):221-34. Epub 2013/04/13. doi: 10.1007/s10822-013-
723 9644-8. PubMed PMID: 23579614.
724 40. Lu C, Wu C, Ghoreishi D, Chen W, Wang L, Damm W, et al. OPLS4: Improving Force
725 Field Accuracy on Challenging Regimes of Chemical Space. J Chem Theory Comput.
726 2021;17(7):4291-300. Epub 2021/06/08. doi: 10.1021/acs.jctc.1c00302. PubMed PMID:
727 34096718.
728 41. Yan Y, Tao H, He J, Huang SY. The HDOCK server for integrated protein-protein
729 docking. Nat Protoc. 2020;15(5):1829-52. Epub 2020/04/10. doi: 10.1038/s41596-020-0312-
730 x. PubMed PMID: 32269383.
731 42. Pallara C, Jimenez-Garcia B, Romero M, Moal IH, Fernandez-Recio J. pyDock scoring
732 for the new modeling challenges in docking: Protein-peptide, homo-multimers, and domain-
733 domain interactions. Proteins. 2017;85(3):487-96. Epub 2016/10/26. doi:
734 10.1002/prot.25184. PubMed PMID: 27701776.
735 43. Kozakov D, Brenke R, Comeau SR, Vajda S. PIPER: an FFT-based protein docking
736 program with pairwise potentials. Proteins. 2006;65(2):392-406. Epub 2006/08/26. doi:
737 10.1002/prot.21117. PubMed PMID: 16933295.
738 44. Lorenzen S, Zhang Y. Identification of near-native structures by clustering protein
739 docking conformations. Proteins. 2007;68(1):187-94. Epub 2007/04/03. doi:
740 10.1002/prot.21442. PubMed PMID: 17397057.
741 45. Zhang L, Cao L, Gao XS, Zheng BY, Deng YQ, Li JX, et al. A proof of concept for
742 neutralizing antibody-guided vaccine design against SARS-CoV-2. Natl Sci Rev.
743 2021;8(8):nwab053. Epub 2021/10/23. doi: 10.1093/nsr/nwab053. PubMed PMID:
744 34676098; PubMed Central PMCID: PMCPMC8083607.
745 46. Shan S, Mok CK, Zhang S, Lan J, Li J, Yang Z, et al. A Potent and Protective Human
746 Neutralizing Antibody Against SARS-CoV-2 Variants. Front Immunol. 2021;12:766821. Epub

747 2021/12/31. doi: 10.3389/fimmu.2021.766821. PubMed PMID: 34966387; PubMed Central
748 PMCID: PMCPMC8710476.
749 47. Callaway HM, Zyla D, Larrous F, de Melo GD, Hastie KM, Avalos RD, et al. Structure of
750 the rabies virus glycoprotein trimer bound to a prefusion-specific neutralizing antibody. Sci
751 Adv. 2022;8(24):eabp9151. Epub 2022/06/18. doi: 10.1126/sciadv.abp9151. PubMed PMID:
752 35714192; PubMed Central PMCID: PMCPMC9205594.
753 48. Wang E, Sun H, Wang J, Wang Z, Liu H, Zhang JZH, et al. End-Point Binding Free
754 Energy Calculation with MM/PBSA and MM/GBSA: Strategies and Applications in Drug
755 Design. Chem Rev. 2019;119(16):9478-508. Epub 2019/06/28. doi:
756 10.1021/acs.chemrev.9b00055. PubMed PMID: 31244000.
757 49. Humphrey W, Dalke A, Schulten K. VMD: visual molecular dynamics. J Mol Graph.
758 1996;14(1):33-8, 27-8. Epub 1996/02/01. doi: 10.1016/0263-7855(96)00018-5. PubMed
759 PMID: 8744570.
760 50. REED LJ, MUENCH H. A SIMPLE METHOD OF ESTIMATING FIFTY PER CENT
761 ENDPOINTS12. American Journal of Epidemiology. 1938;27(3):493-7. doi:
762 10.1093/oxfordjournals.aje.a118408.
763 51. Zhang M, Wang H, Foster ER, Nikolov ZL, Fernando SD, King MD. Binding behavior of
764 spike protein and receptor binding domain of the SARS-CoV-2 virus at different
765 environmental conditions. Sci Rep. 2022;12(1):789. Epub 2022/01/19. doi: 10.1038/s41598-
766 021-04673-y. PubMed PMID: 35039570; PubMed Central PMCID: PMCPMC8763896.
767

768

769 **Figure Legends:**

770 **Figure 1: Cross-reactivity of antibodies and sera raised against SARS-CoV-2 Spike with**
771 **DENV-2 (NGC) proteins.**

772 (A) Confocal, digital images of DENV-2 (NGC) infected C6/36 cells reacted with 4G2,
773 antibodies and sera raised against SARS-CoV-2 after 48 hpi. Cell nuclei are stained with DAPI
774 while the other antibodies are detected using FITC-labeled respective secondary antibodies.

775 (B) Bar graph showing MFI of 4G2, MSer, 1A9, P1R (normalized w.r.t. the respective
776 secondary antibody controls) with standard deviation. Analysis was performed using ImageJ
777 and statistical significance was carried out using One-way ANOVA followed by Dunnett's test
778 in GraphPad Prism 8·4·2. Asterisk (*) indicates statistically significant difference in MFI w.r.t.
779 Rabishield® (Negative control).P value = 0·1234 (ns), 0·0332 (*), 0·0021 (**), 0·0002 (***),
780 <0·0001 (****)

781 (C) Binding kinetics of C8 (DENV-E protein specific) and 1A9 (SARS-CoV-2 spike specific)
782 antibodies with DENV-2 protein E and SARS-CoV-2 spike protein. Antibodies were loaded
783 onto the sensors and serial dilutions of the proteins were used to study binding kinetics. The
784 binding responses were calculated by subtracting data from reference and fitting globally with
785 a 1:1 binding model using ForteBio's Data Analysis software 10·1. The data was considered
786 validated if $\chi 2$ <0·5.

787

788 **Figure 2: ADE of dengue virus infection by the SARS-CoV-2 positive patients' sera in**
789 **K562 cells.**

790 ADE due to convalescent plasma samples collected in the (A)first interval (Samples collected
791 from May 2020- Jan 2021), n=21, (B) second interval (Samples collected from May 2021-June
792 2021), n=17, and (C) third interval (Samples collected from Feb 2022-April 2022), n=10. The
793 bar graph represents an average percentage increase in DENV positive cells w.r.t. VC for each

794 sample with standard deviation for duplicates. Statistical significance was carried out using
795 One-way ANOVA followed by Dunnett's test in GraphPad Prism 8·4·2. Asterisk (*) indicates
796 that the difference between the virus control and the serum samples is statistically significant.
797 P value = 0·1234 (ns), 0·0332 (*), 0·0021 (**), 0·0002 (***), <0·0001 (****)
798 (D) Representative dot plots of patient samples from the first interval (#143, #155), second
799 interval(#96), and third interval (#2, #7). Data was analyzed on FlowJo version 10·8·1.
800
801 **Figure 3: ADE of dengue virus infection by the monoclonal and polyclonal antibodies and**
802 **serum against SARS-CoV-2.**
803 ADE due to (A) anti-spike monoclonal antibodies, M1B, 1A9, and different volumes of MM41
804 (from 2 µl to 6 µl) and anti-spike polyclonal antibody raised in rabbit, P1R, (B) anti-RBD
805 monoclonal antibodies, M4B, and different volumes of M5B (from 2 µl to 6 µl), (C) hamster
806 serum immunized with SARS-CoV-2 spike and negative control (Rabishield®). Statistical
807 significance was calculated using One-way ANOVA followed by Dunnett's test in GraphPad
808 Prism 8·4·2. Asterisk (*) indicates that the difference between the virus control and the serum
809 samples is statistically significant. P value = 0·1234 (ns), 0·0332 (*), 0·0021 (**), 0·0002 (***),
810 <0·0001 (****).
811 (D) Representative dot plots. Data was analyzed using FlowJo version 10·8·1.
812
813 **Figure 4. Computational insights exploring the cross-reactive SARS-CoV-2 antibodies at**
814 **DENV-2 E protein:** (A) Sequence and structural organization of the DENV-2 E dimer (PDB
815 1OAN). (B) Overview of the computational pipeline. (C) The binding free energy in kcal/mol
816 of selected SARS-CoV-2 antibodies. The most likely complexes were generated using Protein-
817 protein dockings. (D) The interaction map of top three antibodies (CR3022: 6W7Y: violet,
818 S2E12 neutralizing antibody Fab fragment: 7K45: orange and DMAb 2196: 8D8R: magenta)

819 along with the native antibody of DENV-2 E as control (C8:4UTA: green). The residue-wise
820 zoom-out view is shown to highlight the critical residues mainly forming the interactions such
821 as Hbonds and SBs. The DENV-2 antibody interactions are shown in green-colored residues
822 and SARS-CoV-2 antibody interactions are highlighted in the pink-colored residues. (E) The
823 matrix of critical residues involved in either establishing either H-bonds or in SBs along with
824 their occurrence. (F) The per-residue decomposition of top three antibodies indicating the
825 thermodynamic contributions of epitope residues. (G) The net binding energy between
826 identified antibodies and DENV-2 E which claims as potential in both cases. (H) The 3D
827 positioning of identified epitope residues at dimer of DENV. The residues which only interact
828 with SARS-CoV-2 antibodies are shown in cyan, the residues interacting with only DENV-2
829 antibody are shown in green color. The residues which are interacting with both DENV-2 E as
830 well as with SARS-CoV-2 RBD are shown in violet color. All the residues are rendered in
831 licorice and atom-wise C:cyan/green/violet, N:blue, O:red and S:yellow.
832
833 **Figure 5: Cross-reactivity and ADE of Dengue virus infection by the SARS-CoV-2 anti-**
834 **RBD antibody CR3022.**
835 (A) Confocal, digital images of DENV-2 (NGC) infected C6/36 cells stained with CR3022
836 along with the controls, 4G2 and Rabishield® (taken from Figure 1 to show the comparison)
837 and the Mean Fluorescence Intensity (MFI).
838 (B) Binding kinetics of CR3022 with SARS-CoV-2 spike protein (i) and DENV-2 protein E
839 (ii).
840 (C) ADE of DENV-2 infection by different concentrations of CR3022 in K562 cells by
841 flowcytometry. Statistical significance was checked using One-way ANOVA followed by
842 Dunnett's test. Asterisk (*) indicates a statistically significant difference between the control
843 and treatment. P value = 0·1234 (ns), 0·0332 (*), 0·0021 (**), 0·0002 (***), <0·0001 (****).

844

845 **Figure 6: Effect of SARS-CoV-2 on dengue infection in AG129 mice:** (A) Schematic
846 experimental plan showing three animal groups: Mock as G1, adeno-ACE-2 viral vector
847 infection at 5 days prior to day 0 in G2 and G3, SARS-CoV-2 infection at day 2 followed by
848 infection with Dengue virus at day 21 in G2, and dengue virus infection at day 21 in G3. (B)
849 Change in body weight. Two-way ANOVA was used. (C) SARS-CoV-2 Spike antibody
850 response at day 21 (D) DENV2 viral particles quantification by FFU assay in the serum of
851 infected mice. Mann-Whitney U test was used for analysis. (E) Dengue viral genome quantified
852 by qRT-PCR from liver, (F) spleen. One-way ANOVA and Bonferroni's post-test were used.
853 PBMC were harvested and (G) platelet count, (H) WBC count, (I) haematocrit percentages
854 were measured. Data are represented as mean ± SEM. *P < 0.05, **P < 0.01, ***P < 0.001,
855 ****P < 0.0001, ns = non-significant.

856

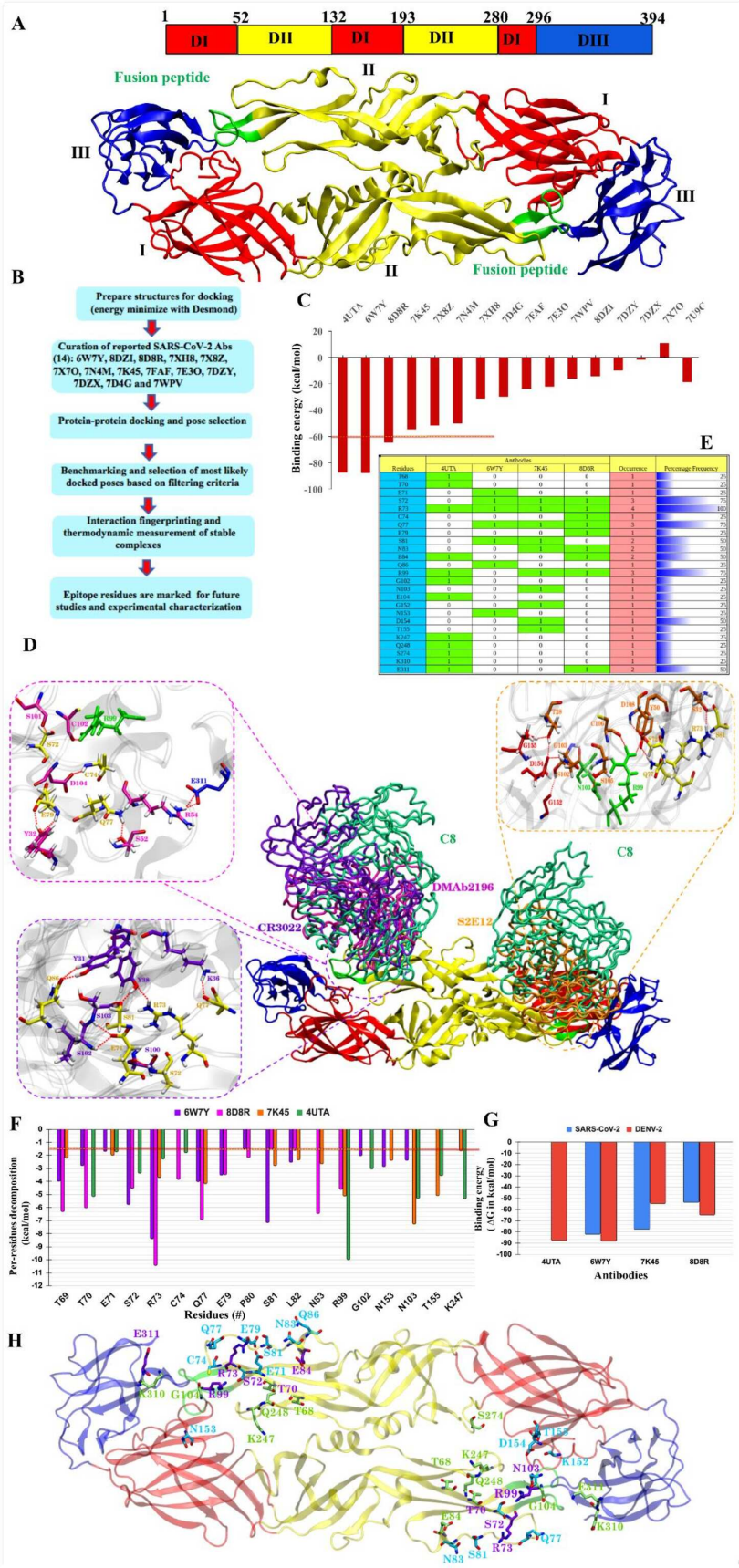
A
1
52
132
193
280
296
394
DI
DII
DI
DII
DI
DIII
Fusion peptide
II
I
III
III
I
II
Fusion peptide
B
Prepare structures for docking (energy minimize with Desmond)
Curation of reported SARS-CoV-2 Abs (14): 6W7Y, 8DZI, 8D8R, 7XH8, 7X8Z, 7X7O, 7N4M, 7K45, 7FAF, 7E3O, 7DZY, 7DZX, 7D4G and 7WPV
Protein-protein docking and pose selection
Benchmarking and selection of most likely docked poses based on filtering criteria
Interaction fingerprinting and thermodynamic measurement of stable complexes
Epitope residues are marked for future studies and experimental characterization
C
4UTA
6W7Y
8D8R
7K45
7X8Z
7N4M
7XH8
7D4G
7FAF
7E3O
7WPV
8DZI
7DZY
7DZX
7X7O
7L9C
Binding energy (kcal/mol)
20
0
-20
-40
-60
-80
-100
E
Antibodies
Residues
4UTA
6W7Y
7K45
8D8R
Occurrence
Percentage Frequency
T68 1 0 0 0 1 25
T70 1 0 0 0 1 25
E71 0 1 0 0 1 25
S72 0 1 1 1 3 75
R73 1 1 1 1 4 100
C74 0 0 0 1 1 25
Q77 0 1 1 1 3 75
E79 0 0 0 1 1 25
S81 0 1 1 0 2 50
N83 0 0 1 1 2 50
E84 1 0 0 1 2 50
Q86 0 1 0 0 1 25
R99 1 0 1 1 3 75
G102 1 0 0 0 1 25
N103 0 0 1 0 1 25
E104 1 0 0 0 1 25
G152 0 0 1 0 1 25
N153 0 1 0 0 1 25
D154 0 0 1 0 1 50
T155 0 0 1 0 1 25
K247 1 0 0 0 1 25
Q248 1 0 0 0 1 25
S274 1 0 0 0 1 25
K310 1 0 0 0 1 25
E311 1 0 0 1 2 50
D
C8
DMAb2196
CR3022
S2E12
C8
F
6W7Y
8D8R
7K45
4UTA
Per-residues decomposition (kcal/mol)
0
-1
-2
-3
-4
-5
-6
-7
-8
-9
-10
-11
-12
T69
T70
E71
S72
R73
C74
Q77
E79
P80
S81
L82
N83
R99
G102
N153
N103
T155
K247
Residues (#)
G
SARS-CoV-2
DENV-2
Binding energy (ΔG in kcal/mol)
0
-10
-20
-30
-40
-50
-60
-70
-80
-90
-100
4UTA
6W7Y
7K45
8D8R
Antibodies
H
E311
Q77
E79
N83
Q86
C74
S81
R73
E71
E84
S72
T70
K310
G104
R99
Q248
T68
N153
K247
S274
D154
T155
K152
T68
K247
N103
Q248
E311
R99
G104
T70
E84
S72
K310
Q77
N83
S81
R73

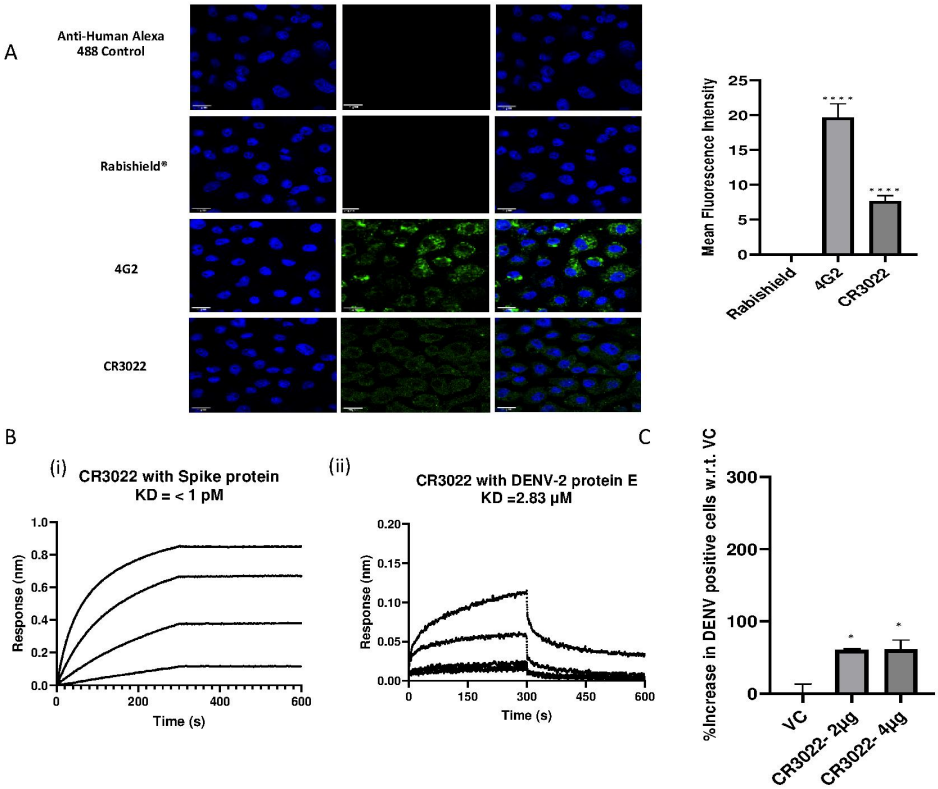
A
Anti-Human Alexa 488 Control
Rabishield®
4G2
CR3022
Mean Fluorescence Intensity
25
20
15
10
5
0
Rabishield
4G2
CR3022
B
(i)
CR3022 with Spike protein
KD = < 1 pM
Response (nm)
Time (s)
(ii)
CR3022 with DENV-2 protein E
KD =2.83 µM
Response (nm)
Time (s)
C
%Increase in DENV positive cells w.r.t. VC
300
200
100
0
VC
CR3022- 2µg
CR3022- 4µg

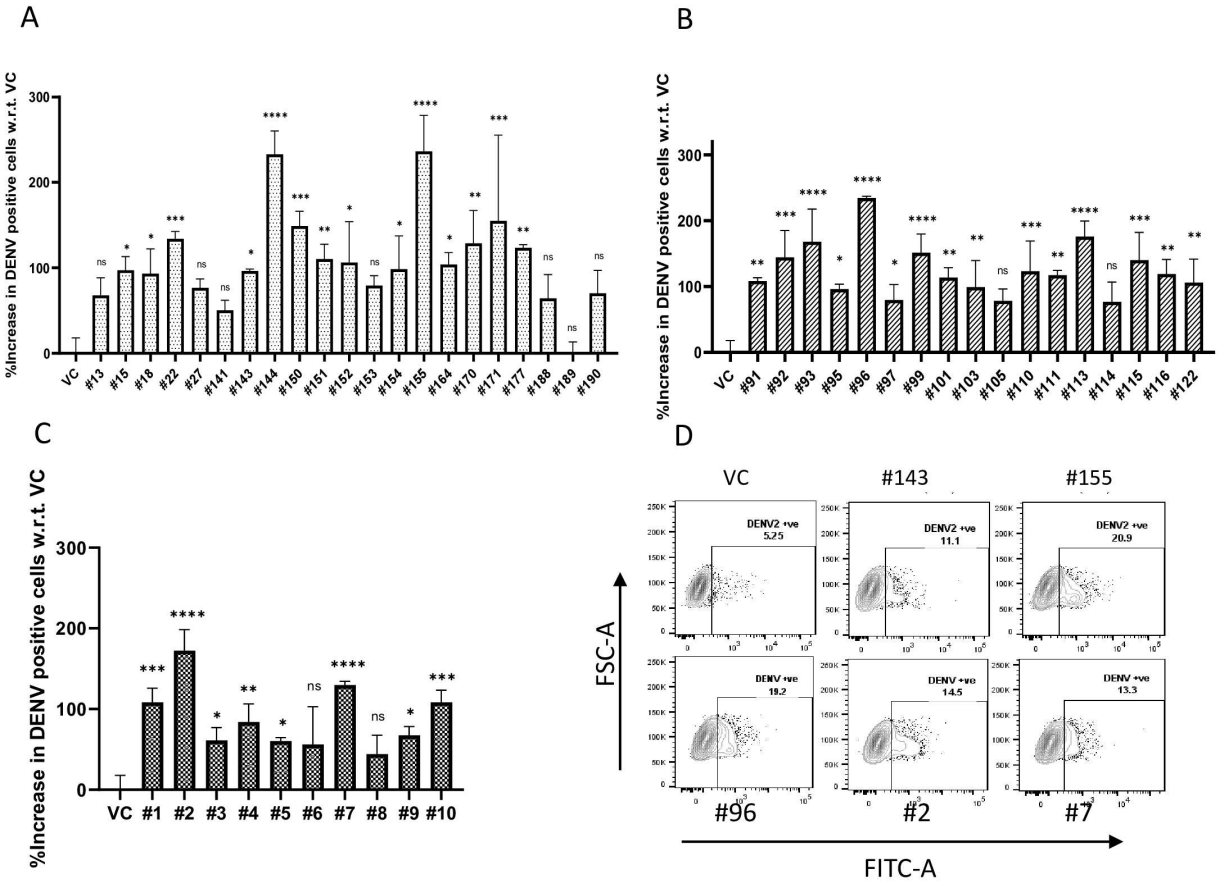
A
%Increase in DENV positive cells w.r.t. VC
300
200
100
0
VC #13 #15 #18 #22 #27 #141 #143 #144 #150 #151 #152 #153 #154 #155 #164 #170 #171 #177 #188 #189 #190
B
%Increase in DENV positive cells w.r.t. VC
300
200
100
0
VC #91 #92 #93 #95 #96 #97 #99 #101 #103 #105 #110 #111 #113 #114 #115 #116 #122
C
%Increase in DENV positive cells w.r.t. VC
300
200
100
0
VC #1 #2 #3 #4 #5 #6 #7 #8 #9 #10
D
VC
#143
#155
DENV2 +ve 5.25
DENV2 +ve 11.1
DENV2 +ve 20.9
DENV +ve 19.2
DENV +ve 14.5
DENV +ve 13.3
FSC-A
#96
#2
#7
FITC-A

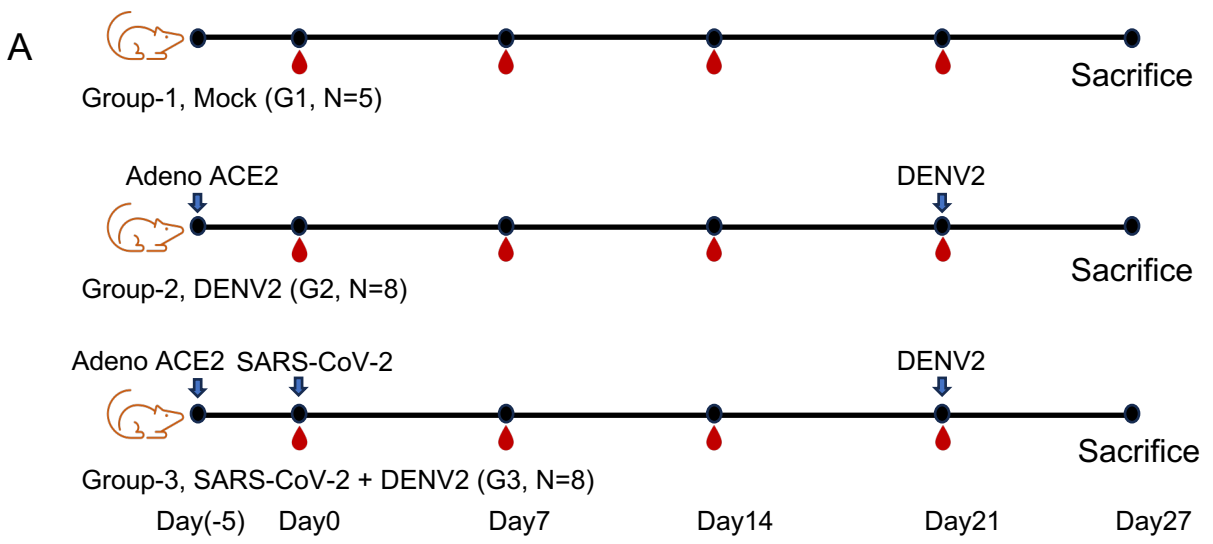
A
Group-1, Mock (G1, N=5)
Sacrifice
Adeno ACE2
DENV2
Group-2, DENV2 (G2, N=8)
Sacrifice
Adeno ACE2
SARS-CoV-2
DENV2
Group-3, SARS-CoV-2 + DENV2 (G3, N=8)
Sacrifice
Day(-5)
Day0
Day7
Day14
Day21
Day27

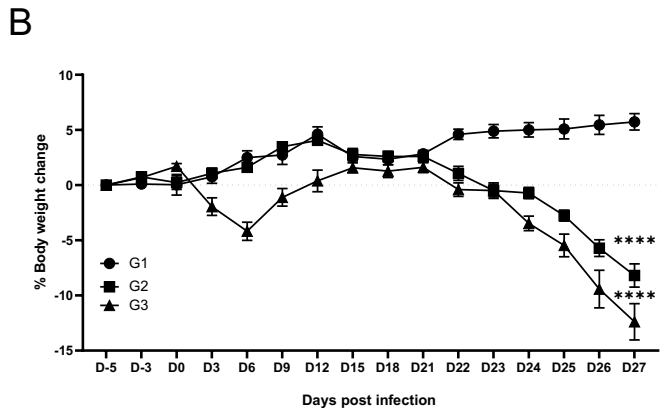
B
% Body weight change
G1
G2
G3
****
****
D-5
D-3
D0
D3
D6
D9
D12
D15
D18
D21
D22
D23
D24
D25
D26
D27
Days post infection

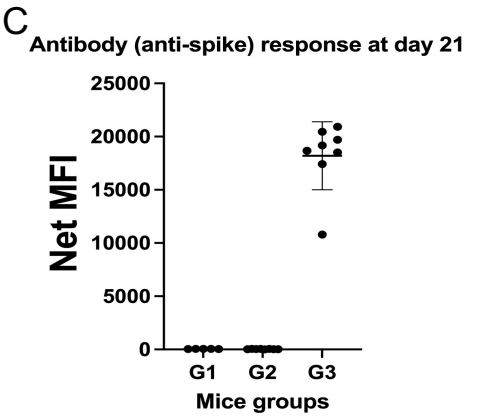
C
Antibody (anti-spike) response at day 21
Net MFI
G1
G2
G3
Mice groups

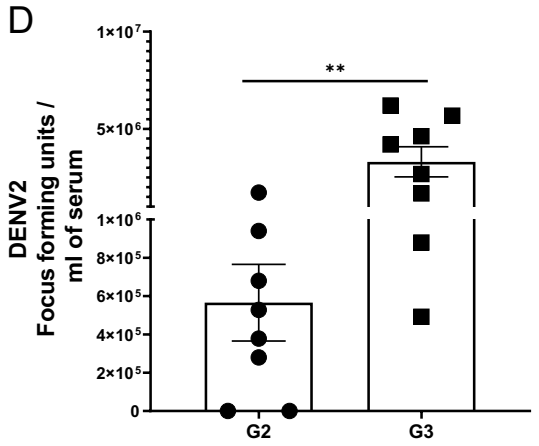
D
DENV2
Focus forming units / ml of serum
**
G2
G3

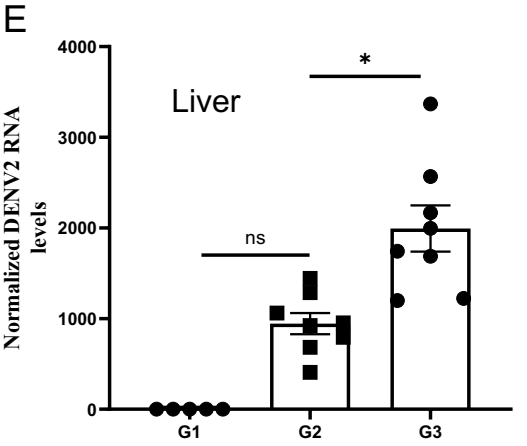
E
Liver
Normalized DENV2 RNA levels
ns
*
G1
G2
G3

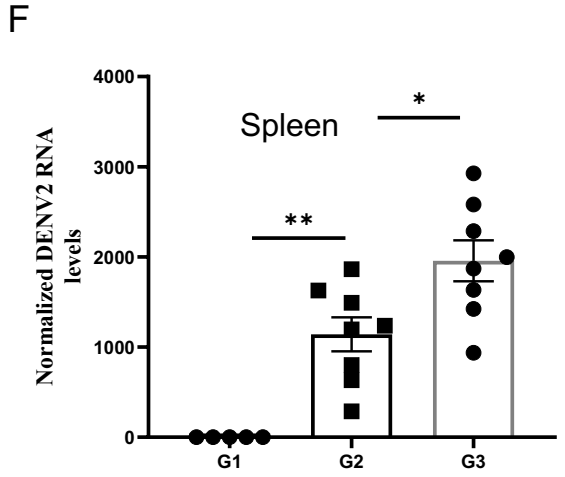
F
Spleen
Normalized DENV2 RNA levels
**
*
G1
G2
G3

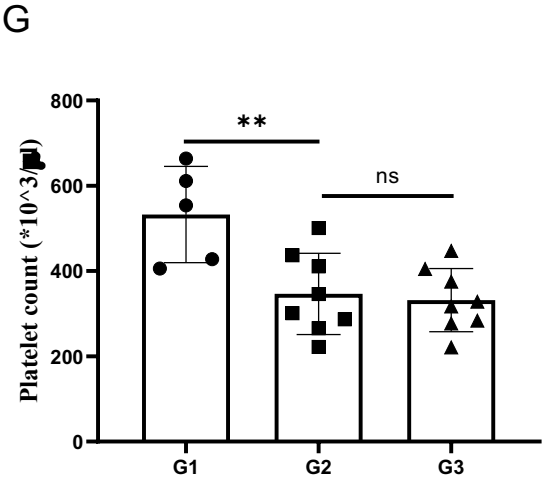
G
Platelet count (*10^3/μl)
**
ns
G1
G2
G3

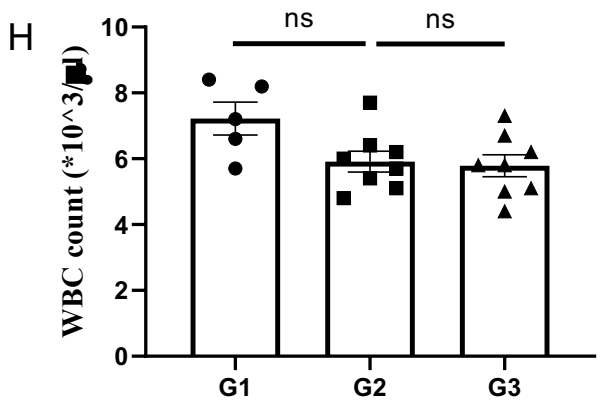
H
WBC count (*10^3/μl)
ns
ns
G1
G2
G3

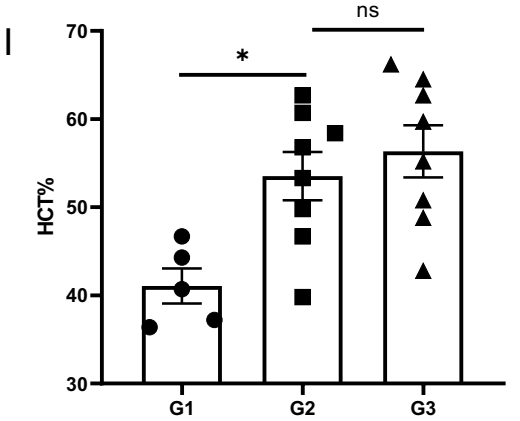
I
HCT%
*
ns
G1
G2
G3

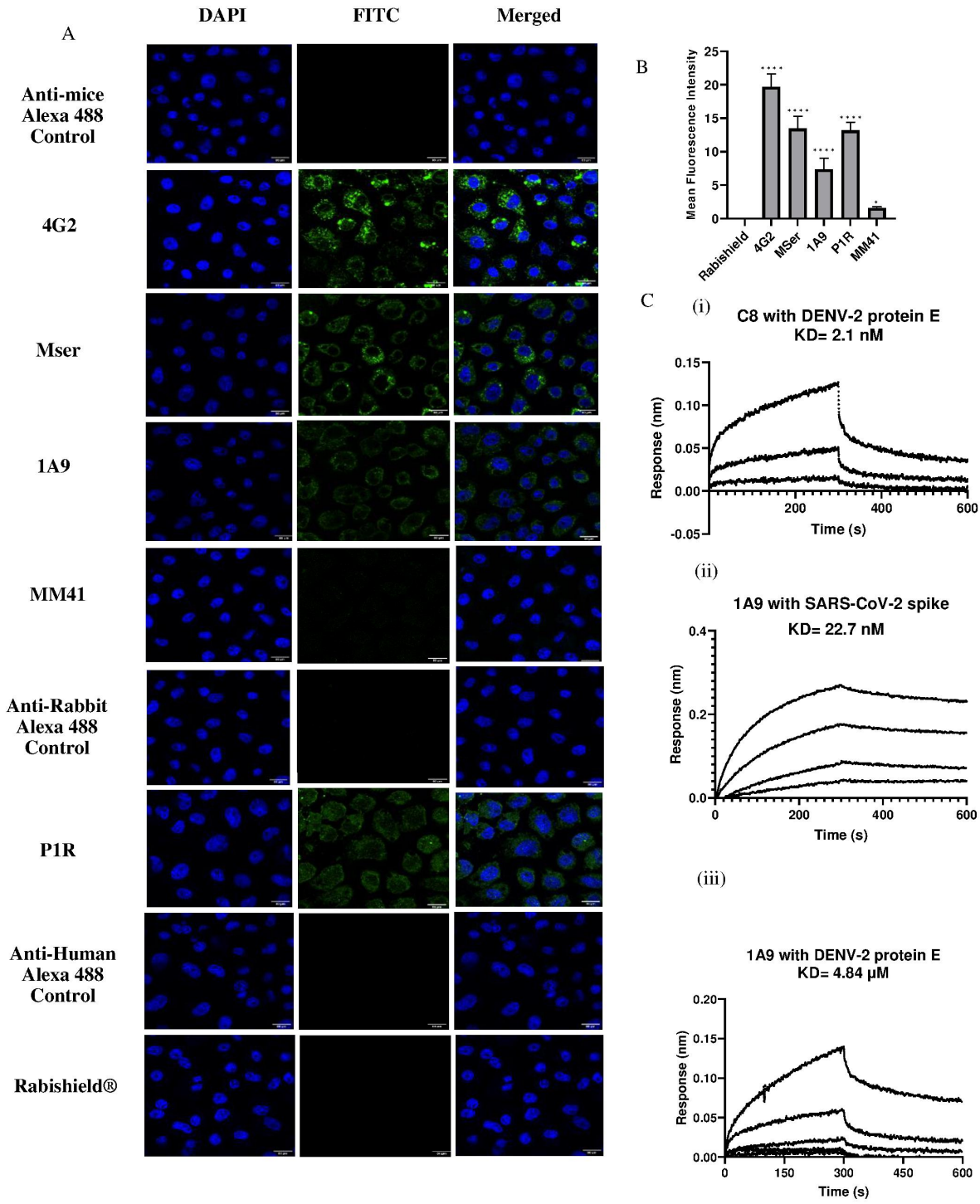
A
DAPI
FITC
Merged
Anti-mice Alexa 488 Control
4G2
Mser
1A9
MM41
Anti-Rabbit Alexa 488 Control
P1R
Anti-Human Alexa 488 Control
Rabishield®
B
Mean Fluorescence Intensity
Rabishield
4G2
MSer
1A9
P1R
MM41
C
(i)
C8 with DENV-2 protein E
KD= 2.1 nM
Response (nm)
Time (s)
(ii)
1A9 with SARS-CoV-2 spike
KD= 22.7 nM
Response (nm)
Time (s)
(iii)
1A9 with DENV-2 protein E
KD= 4.84 μM
Response (nm)
Time (s)

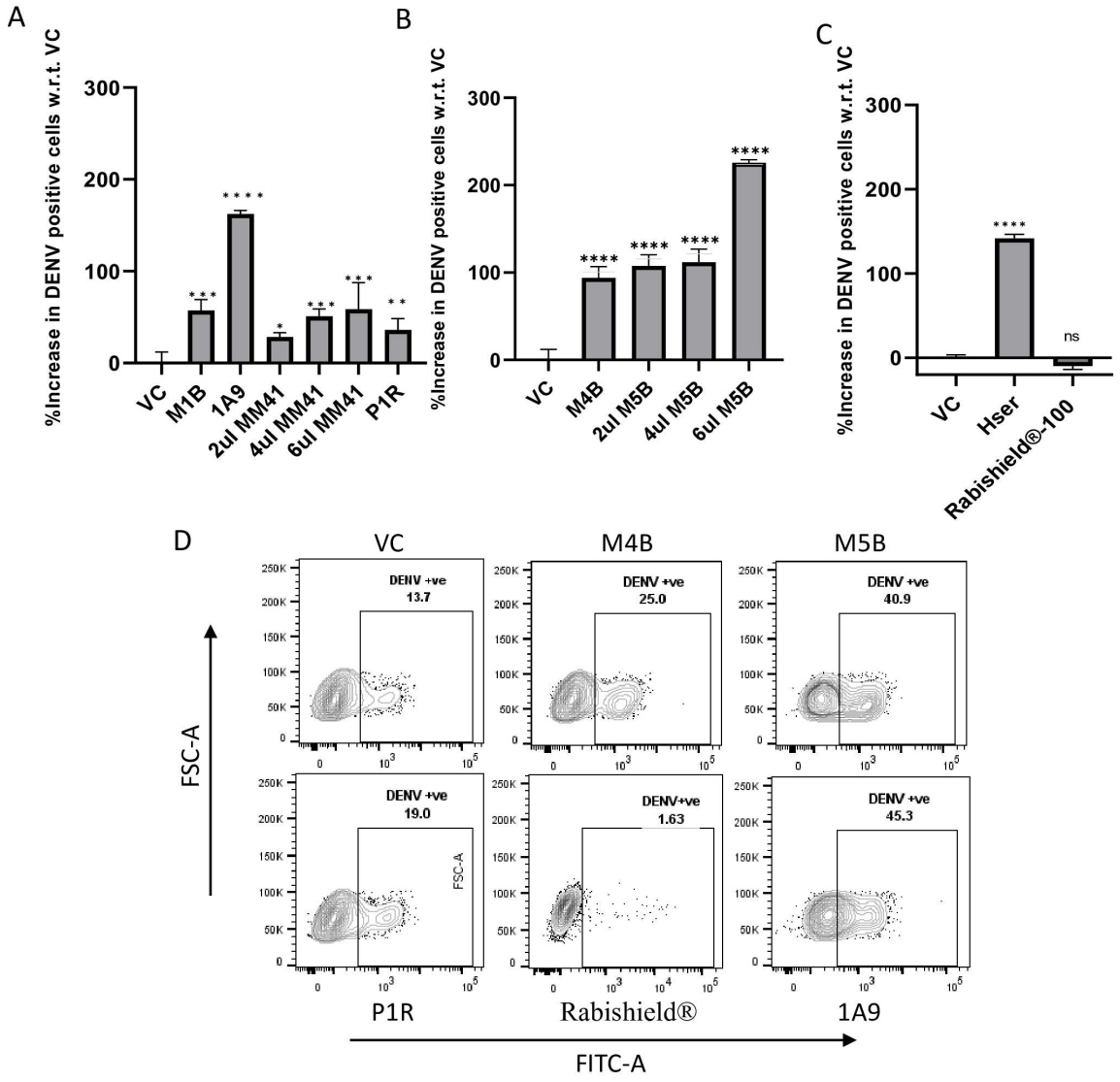
A
%Increase in DENV positive cells w.r.t. VC
300
200
100
0
VC
M1B
1A9
2ul MM41
4ul MM41
6ul MM41
P1R
B
%Increase in DENV positive cells w.r.t. VC
VC
M4B
2ul M5B
4ul M5B
6ul M5B
C
%Increase in DENV positive cells w.r.t. VC
VC
Hser
Rabishield®-100
ns
D
VC
M4B
M5B
DENV +ve 13.7
DENV +ve 25.0
DENV +ve 40.9
DENV +ve 19.0
DENV+ve 1.63
DENV +ve 45.3
FSC-A
P1R
Rabishield®
1A9
FITC-A